A study of inverted-V auroral acceleration mechanisms using Polar/FAST conjunctions

P. Janhunen, [1] A. Olsson, [2,1] W.K. Peterson, [3] H. Laakso, [1] J.S. Pickett, [4] T.I. Pulkkinen, [1] and C.T. Russell [5]

Short title: POLAR/FAST CONJUNCTION STUDY OF INVERTED-V

Abstract. We present observations of electrons and ions that have been affected by an auroral plasma acceleration mechanism. In the nine events studied, nearly simultaneous and magnetically conjugate measurements were made by instruments on the FAST and Polar satellites (1900-4100 and 20000-37000 km altitude ranges, respectively). FAST sees inverted-V type electron spectra in five out of nine events. In cases where the electron distribution at Polar is quasi-Maxwellian (2 events), assuming a potential drop of appropriate magnitude between the two spacecraft can well explain the spectra. In more complicated non-Maxwellian cases (3 events), a net potential drop between FAST and Polar could explain the total FAST energy flux rather well, but not at all the details of the distribution functions. In the remaining four events the precipitation seen at FAST is diffuse rather than inverted-V type. Thus the 'standard' explanation of inverted-V type electron spectra in terms of potential drop acceleration may work in the quasi-Maxwellian events (which represent the small-energy end of inverted-V spectra, with 1-2 keV energies), but not in the non-Maxwellian events. Measurements of the upward flowing ionospheric ions at Polar also supports this view. In the non-Maxwellian events, sporadic very broadband electrostatic wave activity (4-1000 Hz frequency range) temporally well correlates with field-aligned acceleration of the cold (but not the hot) electron population. We suggest that in these cases, the inverted-V energization mechanism is not caused by a potential drop, but is possibly related to the observed correlation of the electron anisotropies and broadband electrostatic wave bursts.

1. Introduction

The U-shaped potential drop (Figure 1) is the standard picture of the electric field structure in auroral inverted-V regions, which first appeared in literature almost 30 years ago [*Carlqvist and Boström,* 1970]. The main evidence for such a potential include (1) an inverted-V shape of precipitating electrons showing downward acceleration [*Evans,* 1974; *Lin and Hoffman,* 1979], and (2) strong (up to 1 V/m) perpendicular electric fields detected in the acceleration region, called electrostatic shocks [*Mozer et al.,* 1977]. Also, upward accelerated ions are often observed within the acceleration region at 1-2 R_E altitude from the Earth's surface [*Shelley and Collin,* 1991], and large upward electric fields have also been directly measured [*Mozer and Kletzing,* 1998]. Conjugate studies between DE 1 and DE 2 satellites [*Reiff et al.,* 1988] generally support this picture as well. Thus, one can say that the U-shaped potential picture is able to account for the most important observational findings below about 12000 km altitude on auroral inverted-V precipitation regions. In geometrically asymmetric cases, the U-shaped (or V-shaped) potential would rather look S-shaped [*Mozer et al.,* 1980].

Figure 1

The success of the U-shaped model to explain observations below 12000 km still leaves open the question whether the upright legs of the U-shaped potential extend up to the equatorial plane (closing only on the opposite hemisphere in a symmetric structure), or whether the potential contours rather close at some altitude which is above 12000 km but below the equatorial plane. A statistical study of Polar electric field data at $\sim 4R_E$ altitude suggested the latter alternative, i.e. that the potential contours often close below 4 R_E altitude in the case of stable arcs [*Janhunen et al.,* 1999].

In this paper we test the U-potential model up to Polar altitude using magnetic conjunctions with FAST. The setup is similar to what Reiff *et al.*[1988] did for DE 1 and DE 2, but we use auroral conjunction events between Polar (20000-37000 km altitude) and FAST (1900-4100 km altitude) so that the altitude range is wider than what was previously explored. Besides particle instruments, we use data from Polar wave detectors to find that the arc-associated electron acceleration in certain types of events is correlated with broadband electrostatic wave bursts.

2. Instrumentation

The Polar satellite was launched in February 24, 1996, into a polar orbit with 9 R_E apogee over the northern hemisphere and 2 R_E perigee over the southern hemisphere. In the examples studies here the northern auroral oval is crossed at about 4 R_E altitude (5 R_E geocentric distance, equivalently).

2.1. HYDRA

The Polar/HYDRA can measure electrons in the 0.01 - 20 keV range [*Scudder et al.,* 1995]. We use 12 second resolution data which have been integrated over 0-30, 75-105 and 150-180 degree pitch angle bins. These bins are called parallel, perpendicular and antiparallel, respectively. The raw count rates of HYDRA are proportional to the differential energy flux, from which we can compute the particle flux and distribution function by dividing by energy and energy squared, respectively. Corrections due to the spacecraft potential are neglected. These corrections might be needed for energies lower than about 50 eV; likewise, at these energies photoelectrons emitted from the satellite, which are also neglected, may also contribute to the measured count rate.

2.2. TIMAS

The Polar/TIMAS (Toroidal Imaging Mass Angle Spectrograph) instrument [*Shelley et al.,* 1995] measures the energy and pitch angle distribution of ions for a wide energy range (15 eV to 32 keV). The instrument can identify four ion species (hydrogen, oxygen and singly and doubly charged helium) and it sweeps through all solid angles in about 3 s (half spacecraft spin). In this paper we study mainly the energy and pitch angle characteristics of outflowing ionospheric ions (we concentrate particularly on oxygen).

2.3. EFI and PWI

Polar electric field instrument data [*Harvey et al.,* 1995] are used to estimate the amplitude of electric waves in the 4-10 Hz frequency range. The plasma wave instrument PWI [*Gurnett et al.,* 1995] onboard Polar uses the same antennas as EFI. Here we study the correlation between

broadband electrostatic wave activity and HYDRA electron anisotropies for wave frequencies above 28 Hz. Together, EFI and PWI cover a wide enough frequency range 4-1000 Hz to contain the interesting waves in this region (the range 10-25 Hz is covered using PWI snapshots only).

2.4. PSI

The Plasma Source Instrument (PSI) [*Moore et al.,* 1995] reduces the spacecraft potential to a few Volts and produces small perturbations at the long wire antennas that affect the DC and AC electric field measurements [*Comfort et al.,* 1998]. Likewise, it may affect the low-energy plasma measurement (the less than 50 eV part of HYDRA). We do not draw any conclusions of the low-energy HYDRA data in this paper, likewise, we do not use DC electric field data from EFI. Possible effects of PSI on PWI are treated in the Observations section below.

2.5. FAST electrostatic analyzer

The electrostatic analyzers onboard FAST [*Carlson et al.,* 1998] measure the distribution functions of electrons in the range 4 eV to 30 keV. The time resolution varies but is typically about 0.3 seconds which corresponds to about 2 km in the ionosphere, which is quite sufficient to characterize the precipitation to the accuracy required in a conjugate study between Polar and FAST.

2.6. CANOPUS magnetometer network

CANOPUS is a ground-based magnetometer network covering central Canada. We use it in six cases to put the event in its geophysical context and to evaluate the magnetic disturbance level. For one event (970608) we use data from the Kotelny Island (KTN) station, which belongs to the "210 magnetic meridian" chain maintained by the Nagoya University.

3. Observations

We searched through all events where Polar and FAST are on the same or nearby magnetic field line above the northern auroral zone. We found five events where inverted-V structures were apparent

in FAST electron data and four conjunctions which had mainly diffuse precipitation at FAST. The times and spacecraft altitudes of the events are given in Table 1. We also present a measure of the quality of the Polar/FAST magnetic conjunctions which we call the smallest equal-time distance. It is the smallest distance between the ionospheric footprints at the same time. Another measure of conjunction quality (not shown) is the time difference when Polar and FAST are passing through particular auroral arcs.

Table 1

For magnetic field line mapping between Polar and FAST we employ the Tsyganenko-95 (T95) model with true dipole tilt, $K_p = 3$, Dst $= 0$ and solar wind dynamic pressure of 2 nPa for the external part and the IGRF model for the internal part. Varying the K_p index or the type of the field model produced only small differences in the ionospheric footpoints.

We also estimate the possible mapping error by another method which takes the maximum magnetic field observed during the event at Polar and subtracts a model magnetic field from it, to obtain a variation field. Assuming that the variation field is due to a field-aligned current, the magnitude of the variation field scales as $\sqrt{B}$ between Polar and the ionosphere. Although we know the direction of the variation vector at Polar, it is difficult to know the direction below the spacecraft. Consequently we compute the mapping error for different directions. Selecting the worst case shows that a mapping error as large as 10 degrees in longitude can be produced by this estimation. In latitude the error is much less. Longitudinal errors in mapping do not matter if the arcs are east-west aligned.

We will use three categories for our events: (1) diffuse Maxwellian events (diffuse precipitation at FAST, approximately Maxwellian spectra at HYDRA), (2) quasi-Maxwellian events (inverted-V precipitation at FAST, approximately Maxwellian HYDRA spectra most of the time), and (3) non-Maxwellian events (inverted-V precipitation at FAST and HYDRA spectra most of the time composed of more than one Maxwellian). Those events that we call "quasi-Maxwellian" here are usually not really Maxwellian in the mathematical sense. Ouf definition is that if a particle spectrum has only a single peak and is not "box-like" (i.e. does not have a wide plateau), it is termed quasi-Maxwellian, otherwise non-Maxwellian in this paper.

Figures 2 and 3 show the locations of the events on the world map and the FAST/Polar mapping

Figures 2 a

for six of the events. The maps are not shown for three diffuse events (980727, 970720, 980811) which are not discussed in much detail below. Table 1 gives the smallest equal-time distance of the ionospheric footpoints, which is one measure of the accuracy of the conjugacy. However, when evaluating the events one must also take into account where the arcs are with respect to the spacecraft at each moment of time (see Figure 3).

To evaluate the stability of the arc events we use ground magnetometers. As a summary, Figure 4 gives a the X component of the closest ground magnetometer station in a 3-hour window around each of the discrete events. Usually the events are rather quiet, but 970603 is a bit more disturbed. We will discuss the ground magnetic data below in connection with the individual events when needed.

3.1. Diffuse precipitation events

In four events (Table 1) the electron precipitation at FAST is mostly of the diffuse type and seemingly coming from a Maxwellian source plasma.

In Figure 5 we show HYDRA and FAST energy fluxes for 970710. After Polar and FAST have been mapped to a common invariant latitude (ionospheric footpoint), they have a time difference which has been indicated by colored dots in the upper panel (see the figure caption for explanation of the coding). The time difference can also be inferred from the numeric UT time labels given in the upper two panels. The integrated energy fluxes (Figure 5, bottom panel) match pretty well (disregarding the energy flux peak in FAST at about 74.5 ILAT which is probably a temporal variation). This serves as a first consistency check for the correctness of the mapping, and it also shows that in the absence of inverted-V type precipitation, the measured energy fluxes by high and low altitude spacecraft are comparable. In the other diffuse events (970720, 980727, 980811) we can also confirm these findings.

Figure 5

Note in passing that although we classify 970710 as diffuse event, there is inverted-V precipitation also, concentrated at 74-75 invariant latitude. Since the time difference is already more than 20 minutes at 74-75 ILAT, however, we do not discuss this aspect of 970710 further in this paper.

FAST energy fluxes tend to be on the average somewhat higher (factor of roughly 2 to 3) than

HYDRA fluxes in all four diffuse events. We do not think that this is an instrumental calibration issue. Anyway, the difference is clearly less than for inverted-V events which are discussed next.

3.2. Quasi-Maxwellian inverted-V events (970615, 970629)

In Figure 6 the HYDRA/FAST energy fluxes mapped into the ionosphere along the magnetic field is plotted against invariant latitude for 970615. We identify three auroral arcs in FAST data which are marked in the figure. Notice that the times increase with decreasing invariant latitude because the satellites are moving southward. For the 970615 event analysis we have shifted the FAST latitude by 0.6 degrees to get better agreement between acceleration features as was done by Reiff *et al.*[1988]; the shift is done in all our data processing concerning event 970615, but not when data are plotted. The need for the shift can come about if the arc is not completely east-west aligned or has moved a little during the event. The integrated energy flux in FAST is clearly higher (at least by an order of magnitude) than in HYDRA during the arc crossings. When the energy flux discrepancy is largest (arc 1) the temporal difference between HYDRA and FAST is more than 15 minutes. During arc 2 and arc 3 the temporal difference is smaller, 5-10 minutes, and the energy flux discrepancy is roughly 10. Figure 6

In event 970629 (data not shown) the energy flux discrepancy is even larger (a factor of about 100), but the temporal difference is also rather large (15-25 minutes).

Figure 7 shows TIMAS ion data for 970615. During arcs 2 and 3 the upgoing oxygen energies are small (less than about 200 eV). There are some oxygen ions at higher energies also, but they have a rather isotropic pitch angle distribution (this cannot be deduced from the figure but we verified it using the data files). At arc 1 the upgoing oxygen has a higher energy, about 1-2 keV. Thus, arc 1 is compatible with a potential drop estimated from the FAST peak, but arcs 2 and 3 are not. The time difference is the largest at arc 1 (and the sign is such that HYDRA measures the region before FAST so that the oxygen time of flight effect (of the order of minutes from FAST to Polar) does not help to reduce the time difference) and becomes better at arcs 2 and 3, so as a whole the 970615 ion data do not show clear evidence for energization of oxygen by a potential drop. Figure 7

For 970629 (data not shown), TIMAS data show that there is outflowing oxygen whose energy (again up to 2 keV) is qualitatively in agreement with the FAST peak energy. Thus the oxygen ions in this event are compatible with a potential drop of 1-2 kV.

The velocity of 1 keV oxygen ions is about 1 R_E per minute and Polar is about 2 R_E above the auroral acceleration region. Thus, the conclusions drawn from the oxygen data are subject to the constraint that the arcs remain stationary for a few minutes at least, which is an assumption we are making in any case.

3.3. Non-Maxwellian inverted-V events (970603, 970606, 970608)

Event 970603 takes place over the northern coastline of Alaska and Canada, and from CANOPUS data (not shown in detail) we see that there is a substorm going on close to FCHU. The nearest CANOPUS stations DAWS and CONT show about 200 nT variations (Figure 4), which can well be due to the substorm current systems (that is, not produced locally). Event 970606 is also located in the arctic Canada, and the conditions are quiet as judged from CANOPUS data (Figure 4). The temporal mapping between Polar and FAST is close to optimal for 970603. By optimal mapping we mean that zero temporal difference occurs at some of the arcs. The temporal mapping in event 970606 is not quite optimal (time difference is more than 9 min). Event 970608 happens over northeastern Siberia and is likewise magnetically rather quiet (Figure 4). This event has good mapping (2-10 minutes time difference during the arcs; concerning the time differences, see the colored dots in the panels).

Figures 8 and 9 show HYDRA and FAST energy fluxes for 970603 and 970606, respectively. In both cases, the energy flux at FAST is the same as or larger (sometimes much larger) than that at Polar. During the discrete arcs when inverted-V precipitation can be seen, FAST energy flux is typically about 10 times higher than HYDRA energy flux.

Figures 8 a

By computing the ratio of the HYDRA distribution function in the parallel and perpendicular directions we can get an estimate of the anisotropy of the distribution. Figures 10 and 11 show this anisotropy for 970603 and 970606, respectively, together with wave amplitudes summed from the PWI

Figures 10 a

and EFI instruments (which use the same sensors) over two frequency bands, 4-10 Hz (EFI) and 28-1000 Hz (PWI) averaged over 10 seconds. We see in Figures 10 and 11 a clear temporal correlation between HYDRA anisotropies and EFI+PWI wave power. For PWI, we used the longest boom (U) data only. We see that the most important electrostatic wave activity is very bursty and occurs below 1 kHz. In all our non-Maxwellian events, the Plasma Source Instrument (PSI) onboard Polar is on. The PSI operation does create spurious waves in the surroundings of the spacecraft, and one must be very cautious when interpreting wave data. In general, the effect of PSI on PWI is to raise the background noise level in the electric measurements at all frequencies up to a few hundred kHz. However, in our events we see no plausible mechanism for how PSI could cause the observed strong electrostatic wave bursts in correlation with HYDRA electron anisotropies. As a further check, we have also looked at some other examples of Polar data where PSI is off, and similar correlated occurrences of anisotropies and wave bursts were found in several occasions.

Besides monitoring > 28 Hz frequencies all the time, the PWI instrument also takes low-frequency "snapshots" of < 25 Hz waves using all antenna booms (data not shown). A snapshot lasts about 2.5 seconds, and about two snapshots are taken per minute. The snapshots reveal significant burst-type wave activity in the 10-25 Hz frequency range, which is not covered by the EFI and PWI plots in Figures 10 and 11. In fact, a substantial portion of the total spectral power may lie in the 10-25 Hz band. Significant wave activity is seen both in the spin plane and parallel to the spin axis in the low-frequency snapshot band. As a summary, we believe that the wave amplitudes shown in Figures 10 and 11 are underestimates of the true electric wave power in the full 4-1000 Hz frequency range, but the overall qualitative behavior of the wave power as a function of invariant latitude can be trusted, which is enough to infer the abovementioned correlation with HYDRA anisotropies.

In 970603, at arc 2 (Figure 10), a detailed look at HYDRA data reveals clearly superposed Maxwellians during the whole inverted-V arc (not shown). Almost all the time there is $f_{\parallel} > f_{\perp}$ anisotropy and wave activity. At arc 1 we have superposed Maxwellians as well, and we see that when the anisotropy moves to somewhat higher energy (up to a few hundred eV), the wave activity

also intensifies and seems to move to somewhat higher frequency (PWI intensifies relative to EFI). The largest anisotropy occurs at ILAT=70.4, which is a clearly identifiable peak in PWI wave data. The correlation between anisotropy and waves occurs also in the other non-Maxwellian event, 970606 (Figure 11).

Figure 12 shows TIMAS ion data for 970606. During the arcs the energy of the outflowing oxygen is small (<200 eV), except for one brief appearance of 1-2 keV ions at 05:45 UT, but the pitch angles of these higher energy oxygen ions are roughly perpendicular (in addition to Figure 12 we checked it also from the data files where the fluxes are stored as functions of both pitch angle and energy). The time difference is favourable for detecting ions because HYDRA measures the region a few minutes after FAST for arc 1 (for arc 2 the time difference is larger than 10 minutes). From the FAST peak one would expect to find 1-2 keV upgoing oxygen with mostly parallel energy, if the FAST peak is produced by a potential drop between the FAST and Polar altitudes. Figure 12

In event 970603 (TIMAS data not shown) there is a low-energy (<200 eV) upgoing oxygen population during arc 2, and simultaneously a higher energy one (around 2-5 keV) whose intensity is however smaller. The more energetic population is extended over all pitch angles (this was again checked from the data files), however, and therefore does not represent an upgoing beam. The existence of two upgoing oxygen populations at different energies does not really speak in favour of a static potential drop of either magnitude (the magnitude would anyway not correspond to the peak energy in FAST, which is 5-8 kV) but probably indicates the existence of temporal variations and/or inductive-type downward parallel electric fields which accelete oxygen ions sporadically and locally. During arc 1 there is an upgoing oxygen population at 1 keV. The FAST peak is at 3 kV in this case.

In event 970608 (data not shown) only low energy oxygen is seen where the time difference is small between FAST and Polar observations. Thus, neither in this case the oxygen data support the existence of a U-shaped potential drop.

4. Summary of observations

One must note that the set of nine Polar/FAST conjunctions all took place during summertime, and most in June 1997. Thus, the set of conjunctions is not completely representative with respect to season. No clear correlations with Polar altitude can be seen in our nine events.

The major observational findings are:

1. Events could be easily classified as diffuse events, quasi-Maxwellian events, and non-Maxwellian events. (For the definitions of quasi-Maxwellian and non-Maxwellian events, see the beginning part of the Observations section.)

2. In diffuse precipitation events, FAST and HYDRA energy fluxes generally match rather well. The diffuse events show that the mapping method is feasible and provide an independent consistency check for the correctness of the energy flux computation routines for the two spacecraft.

3. During inverted-V electron precipitation (quasi-Maxwellian and non-Maxwellian events), FAST energy flux is typically about 10 times higher than HYDRA energy flux. This demonstrates that, as expected, electron energization below Polar is clearly needed to explain inverted-V events.

4. The two quasi-Maxwellian events show a mixed character. In one event (970615), matching of the spectra and the integrated energy flux is rather good after acceleration through the FAST peak energy (for a quantitative treatment, see the next section). In the other event (970629) the electron matching is not as good, but on the other hand it was found that the energy (1-2 kV) of outflowing O^+ approximately matches the FAST peak energy. Thus, it is unclear whether the events are compatible with small (1-2 kV) potential drops, but in any case there is no evidence for potential drops larger than 1-2 kV among the quasi-Maxwellian events.

5. In the non-Maxwellian events, there is a good temporal correlation between short-lived (or spatially compact) electron anisotropy occurrences at middle ($\sim$ 40-400 eV) energies and broadband electrostatic wave bursts in the 4 Hz $-$ 1 kHz frequency range. The oxygen data do not support a potential drop of similar magnitude as FAST electrons would indicate.

5. Quantitative comparison of FAST and HYDRA electron fluxes

In this section we compare FAST and HYDRA electron fluxes quantitatively. We also test the parallel potential drop model by computing the distribution function from HYDRA, estimating the potential drop V from the particle flux peak position of the conjugate FAST measurement, accelerating the HYDRA distribution by V, and comparing with FAST.

5.1. Quasi-Maxwellian events

In Figure 13 we present 8 examples of HYDRA spectra taken during inverted-V precipitation of 970615. To produce Figure 13 we have simulated the electron spectra that would be obtained if the HYDRA data were accelerated through a potential drop [*Evans,* 1974] that was determined from the corresponding FAST electron data by finding the peak position. A latitudinal shift of 0.6 degree is included in this event in order to improve the correspondence as stated before. The unaccelerated (observed) HYDRA spectra are also shown as the left member of each pair of plots for comparison. The HYDRA spectra have a quasi-Maxwellian character (possibly accelerated by a few tens of eV), while FAST spectra during the discrete arcs show an inverted-V type signature where the peak is around 1 keV. The accelerated HYDRA spectra match with FAST spectra rather well in this case. Figure 13

For the other quasi-Maxwellian event 970629 (Figure 14) the HYDRA electrons are colder and do not produce an equally good match after accelerating them by the FAST peak potential. The HYDRA spectra are deformed a bit from a Maxwellian shape, which adds to the narrowness of the spectra after acceleration so that they fail to reproduce measured FAST spectra to some extent. If the energization is due to a potential drop in 970629, some nonadiabatic process has to broaden the spectra before the particles reach FAST altitude. Figure 14

In Figure 15 we show the accelerated HYDRA energy flux (which should simulate FAST energy flux if the potential drop model is valid) for 970615 for all data points as a spectrogram plot. Comparison with the unaccelerated version (Figure 15, bottom panel, dotted blue line) shows that letting HYDRA electrons go through a potential drop causes energization which improves the correspondence with Figure 15

FAST energy flux, which is not unexpected. Notice that the shift of 0.6 degrees should be done in the bottom panel of Figure 15.

For 970629 (Figure 16) the match after acceleration is not as good as for 970615, as noted above. Figure 16
The coldness of the HYDRA population and its slightly deformation from a Maxwellian character makes the energy flux after acceleration too small in this case.

5.2. Non-Maxwellian events

In Figures 17 and 18 we show the effect of potential drop acceleration on HYDRA data in the Figures 17 a
non-Maxwellian event of 970603. The spectral curves (Figure 17) show that the matching of HYDRA and FAST spectra cannot be very good because HYDRA data consist of two or more peaks, while FAST has only a single peak (there is sometimes a second peak also in FAST but at too low energy to be significant in this regard). The small energy peak of HYDRA, after accelerated through a potential drop, becomes a peak at the correct location (by construction, because the accelerating potential was taken from FAST), but it is far too narrow and too high. Likewise, the higher energy peak of HYDRA becomes a smaller peak at somewhat higher energy, which is absent in the FAST data. In other words, the integrated energy fluxes (Figure 18, bottom panel) match rather well, but the matching of the functional form of the spectra is rather poor. The point is not only that the functional forms mismatch in these particular events, but also that the multiply-peaked HYDRA spectra produce very abnormal-looking inverted-V spectra if accelerated through a potential drop. Thus, questions such as mapping errors and temporal stability which are always a concern in conjunction studies do not affect this conclusion.

The fact that the integrated energy fluxes match after acceleration is not very surprising and should not be taken as an indication that the real energization process is necessarily a potential drop. Especially when the FAST peak energy V is clearly larger than the source plasma thermal energy T, variations in V cause corresponding variations in the accelerated energy flux, almost regardless of how the original HYDRA data look like. This is because the energy flux is under these conditions

approximately proportional to $nT^{-1/2}V^2$ where n is the source plasma density [*Fridman and Lemaire,* 1980]. The energy flux is much more sensitive to variations in V, which is determined by FAST data alone, than to variations in n or T, which are determined by HYDRA data.

The other non-Maxwellian events show a similar behavior as 970603.

Regarding the role of the observed correlation between very broadband electrostatic waves (4-1000 Hz) and middle-energy electron anisotropy, the question arises whether the waves cause the anisotropy or vice versa. We think it more likely that the waves cause the anisotropy, because it is difficult to explain the energy-selective parallel acceleration and the anisotropy by something else than waves. A plausible candidate for the free energy source of the waves is a hot ion population of about 30-50 keV thermal energy. This population is mostly beyond the energy range of HYDRA ion detector, but can be seen in CAMMICE data (not shown). Studying possible plasma instabilities which could tap energy from the hot ion population in the presence of the observed cold and middle-energy populations would be interesting but is beyond the scope of this paper. Assuming the existence of the observed waves at Polar, we have recently shown using test particle simulations that realistic low-altitude inverted-V electron spectra are produced if an O-shaped potential well is assumed to lie between Polar and FAST [*Janhunen and Olsson,* 2000]. This result is compatible with the observations reported in the present paper, and also with the statistical results presented earlier [*Janhunen et al.,* 1999].

6. Comparison with an earlier study

Reiff *et al.* [1988] used similar methods to study acceleration between DE 1 and DE 2 satellites. A difference between their study and ours is that their upper satellite (DE 1) is at 11000-17000 km altitude, whereas ours (Polar) is at 20000-37000 km (Table 1). Therefore, it is not meaningful to compare these two studies in detail, especially as we have shown earlier that acceleration region ($\sim$ 6000-12000 km) potential structures above stable arcs do not usually reach the Polar altitude [*Janhunen et al.,* 1999]. We anyway wish to point out that Figure 15 in Reiff *et al.* [1988] shows a comparison of average upward ion energy $\langle E \rangle_i$ with other estimates of the potential drop $e\Phi_{\mathrm{MID}}$ and

$e\Phi_{\rm TOT}$, where $\Phi_{\rm MID}$ is the potential drop below DE 1, calculated from the loss cone width, and $\Phi_{\rm TOT}$ is the potential drop above DE 2, inferred from the peak electron energy. The quantity that should be compared with the potential drop is $E_{\rm peak}$, plotted in their Figure 14, rather than $\langle E \rangle_i$, as they point out in the text. $E_{\rm peak}$ is usually less than the other estimates of the potential drop, especially in the events where the energies are generally higher. Indeed, $E_{\rm peak}$ never exceeds 3 keV in their events and is usually 1-2 keV at most. Thus, they do not show an example where the ion data would support a *significant* (more than 5 keV) potential drop below the spacecraft. This result is in agreement with ours, despite the difference in spacecraft altitude range.

7. Conclusions

We studied the inverted-V electron acceleration mechanisms between FAST and Polar altitudes. Nine Polar/FAST magnetic conjunction events were found, out of which five contained inverted-V type precipitation. In the inverted-V events the energy flux at FAST was about 10 times higher than the energy flux at Polar so that an energization mechanism is needed. In cases where the electron distribution at Polar is quasi-Maxwellian (2 events), a U-shaped potential drop can explain the electron spectra reasonably well. In more complicated non-Maxwellian cases (3 events) a U-shaped potential could explain the total electron energy flux rather well, but not the details of the distribution functions. In the non-Maxwellian events, a correlation between a middle-energy electron anisotropy and the occurrence of broadband electrostatic waves at Polar is seen.

The quasi-Maxwellian events represent the low-energy end of inverted-V events. They partly support and partly do not support the presence of a potential drop; the potential drop, if it exists, is in any case small (1-2 kV). The non-Maxwellian events have higher peak energies and thus represent the most typical inverted-V events. In these cases, a potential drop model of auroral energization leads to inconsistencies with the spectral shape of precipitating electrons and missing energization of upflowing oxygen, while it can reproduce the integrated precipitating electron energy flux magnitude rather well. We suggest that the energization mechanism in the non-Maxwellian events is rather related to the

observed correlation between electron anisotropies and broadband electrostatic wave bursts.

Acknowledgements We are grateful to Forrest Mozer for providing EFI data and valuable comments, James McFadden and Chuck Carlson for providing the FAST data and some interpretation hints, Craig Kletzing for the HYDRA data and useful comments, Terry Hughes for providing the CANOPUS data, and Kiyohumi Yumoto for Kotelny Island data of the 210 MM project. We also thank many other colleagues for discussions about the topic and practical help. Annika Olsson's work was partly supported by the Knut and Alice Wallenberg Foundation. WKB thanks Dan Baker and LASP for their hospitality during his stays and acknowledges support from NASA under contract NAS5-30302 (Lockheed). The work at UCLA was supported by the NASA grant NAG5-7721. HL is partly supported by the Polar EFI Research Grant to Goddard Space Flight Center (code 696) under NASA grant NAG5-2231. JSP acknowledges support from NASA/GSFC under contract NAS5-30371 and grant NAG5-7943. Craig Kletzing's work is supported by grants NAG5-2231 and DARA 50-0C89110.

References

Carlqvist, P. and R. Boström, Space-charge regions above the aurora, *J. Geophys. Res., 75,* 7140–7146, 1970.

Carlson, C.W., R.F. Pfaff and J.G. Watzin, The Fast auroral snapshot mission, *Geophys. Res. Lett., 25,* 2013–2016, 1998.

Comfort, R.H., T.E. Moore, P.D. Craven, C.J. Pollock, F.S. Mozer, and W.S. Williamson, Spacecraft potential control by the Plasma Source Instrument on the POLAR satellite, J. Spacecraft & Rockets, 845, 1998.

Evans, D.S., Precipitating electron fluxes formed by a magnetic field aligned potential difference, *J. Geophys. Res., 79,* 2853–2858, 1974.

Fridman, M., and J. Lemaire, Relationship between auroral electron fluxes and field aligned electric potential differences, *J. Geophys. Res. 85*, 664-670, 1980.

Gurnett, D.A., A. M. Persoon, R. F. Randall, D. L. Odem, S. L. Remington, T. F. Averkamp, M. M. DeBower, G. B. Hospodarsky, R. L. Huff, D. L. Kirchner, M. A. Mitchell, B. T. Pham, J. R. Phillips, W. J. Schintler, P. Sheyko, and D. Tomash, The Polar Plasma Wave Instrument, Space Sci. Rev., ed. by C. T. Russell, Kluwer Academic Publishers, 71, pp. 597-622, 1995.

Harvey, P., F.S. Mozer, D. Pankow, J. Wygant, N.C. Maynard, H. Singer, W. Sullivan, P.B. Anderson, R. Pfaff, T. Aggson, A. Pedersen, C.G. Falthammar and P. Tanskanen, The electric field instrument on the polar satellite, Space Science Reviews 71, 583-596, 1995.

Janhunen, P., A. Olsson, F.S. Mozer and H. Laakso, How does the U-shaped potential close above the acceleration region? A study using Polar data, *Ann. Geophysicae,* in press, 1999.

Janhunen, P. and A. Olsson, New model for auroral acceleration: O-shaped potential structure cooperating with waves, *Ann. Geophysicae,* in press, 2000.

Lin, C.S, and R.A. Hoffman, Characteristics of the inverted-V event, *J. Geophys. Res., 84,* 1514-1525, 1979.

Moore, T.E., C.R. Chappell, M.O. Chandler, S.A. Fields, C.J. Pollock, D.L. Reasoner, D.T. Young, J.L. Burch, N. Eaker, J.H. Waite, Jr., D.J. McComas, J.E. Nordholt, M.F. Thomsen, J.J. Berthelier and R. Robson, The Thermal Ion Dynamics Experiment and Plasma Source Instrument, Space Sci. Revs., 71, 409, 1995.

Mozer, F.S., C.W. Carlson, M.K. Hudson, R.B. Torbert, B. Parady, I. Yatteau and M.C. Kelley, Observations of paired electrostatic shocks in the polar magnetosphere, *Phys. Rev. Lett.,* 38, 292, 1977.

Mozer, F.S., C.A. Cattell, M.K. Hudson, R.L. Lysak, M. Temerin, and R.B. Torbert, Satellite measurements and theories of low altitude auroral particle acceleration, *Space Sci. Rev., 27,* 155–213, 1980.

Mozer, F.S., and C.A. Kletzing, Direct observation of large, quasi-static, parallel electric fields in the auroral acceleration region, *Geophys. Res. Lett., 25,* 1629–1632, 1998.

Reiff, P.H., H.L. Collin, J.D. Craven, J.L. Burch, J.D. Winningham, E.G. Shelley, L.A. Frank and M.A. Friedman, Determination of auroral electrostatic potentials using high- and low-altitude particle distributions, *J. Geophys. Res., 93,* 7441–7465, 1988.

Scudder, J.D., *et al.*, Hydra - A 3-dimensional electron and ion hot plasma instrument for the Polar spacecraft of the GGS mission, *Space Sci. Rev.,* **71**, 459-495, 1995.

Shelley, E.G. and H.L. Collin, Auroral ion acceleration and its relationship to ion composition, in Auroral physics, Meng, Rycroft and Frank (eds.), Cambridge University Press, 1991.

Shelley, E.G., A.G. Ghielmetti, H. Balsiger, R.K. Black, J.A. Bowles, R.P. Bowman, O. Bratschi, J.L. Burch, C.W. Carlson, A.J. Coker, J.F. Drake, J. Fischer, J. Geiss, A. Johnstone, D.L. Kloza, O.W. Lennartsson, A.L. Magoncelli, G. Paschmann, W.K. Peterson, H. Rosenbauer, T.C. Sanders, M. Steinacher, D.M. Walton, B.A. Whalen

and D.T. Young, The Toroidal Imaging Mass-Angle Spectrograph (TIMAS) for the Polar Mission, Space Science Rev., 71, 1-4, 1995.

P. Janhunen, H. Laakso and T.I. Pulkkinen, Finnish Meteorological Institute, Geophysical Research, P.O.B. 503, FIN-00101, Helsinki, Finland. (e-mail: Pekka.Janhunen@fmi.fi)

A. Olsson, Swedish Institute of Space Physics, Uppsala Division, S-755 91 Uppsala, Sweden. (e-mail: ao@irfu.se)

J.S. Pickett, The University of Iowa, Department of Physics and Astronomy, Iowa City, IA 52242-1479 (e-mail: cak@space-theory.physics.uiowa.edu)

W.K. Peterson, Lockheed Martin Space Sciences Laboratory, Temporary address: LASP 1234 Innovation Drive, Boulder, CO 80303 (e-mail: pete@willow.colorado.edu)

C.T. Russell, Institute of Geophysics and Planetary Physics, University of California at Los Angeles, Los Angeles, CA 90024-1567 (e-mail: ctrussel@igpp.ucla.edu

Received 1999; revised ????; accepted ????.

---

[1]Finnish Meteorological Institute, Helsinki, Finland.

[2]Swedish Institute of Space Physics, Uppsala Division, Uppsala, Sweden.

[3]Lockheed Martin Space Physics Laboratory, Palo Alto, California.

[4]Department of Physics and Astronomy, University of Iowa.

[5]Institute of Geophysics and Planetary Physics, University of California at Los Angeles.

Submitted to *Journal of Geophysical Research*, 1999.

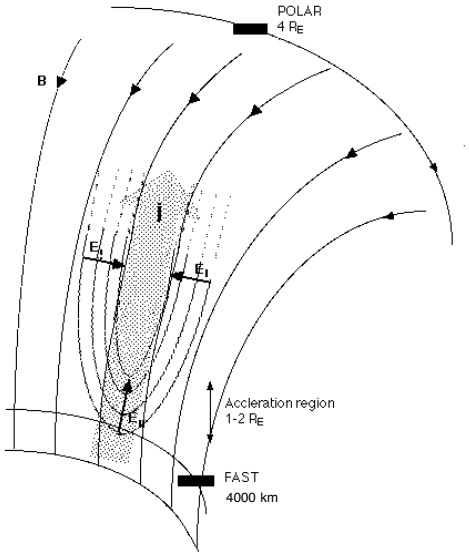

Figure 1. The upward extended U-shaped potential model for auroral electric fields. The acceleration region resides in the $1 - 2R_E$ altitude range. Polar measures the electric field above the acceleration region at about $4R_E$ altitude.

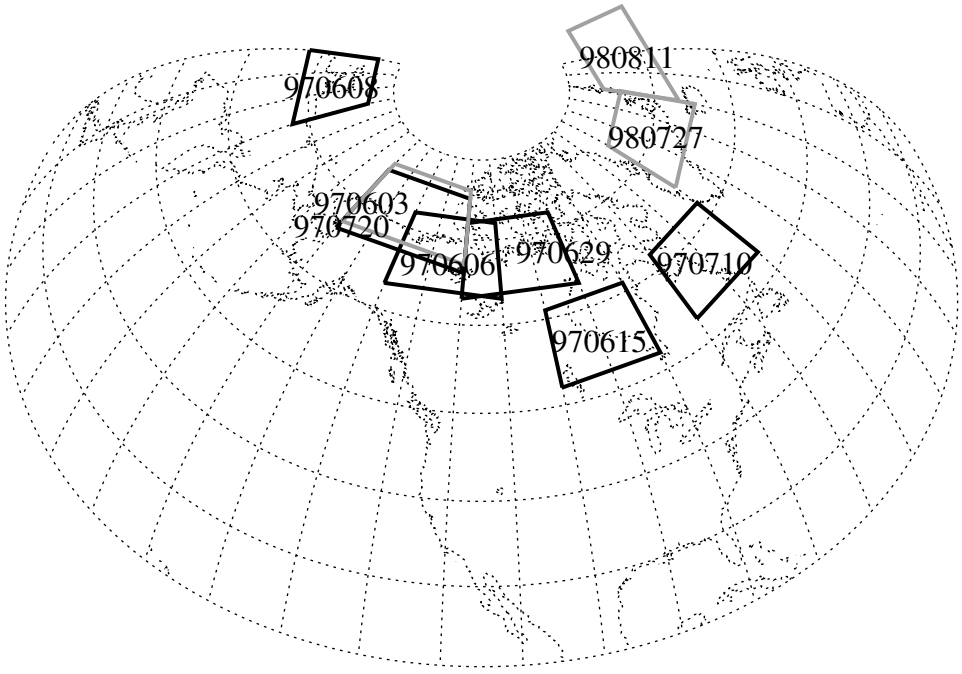

Figure 2. Summary plot of all nine events. The events marked with black boxes are shown in more detail in Figure 3 below while the gray ones are not. All the events marked gray are diffuse events.

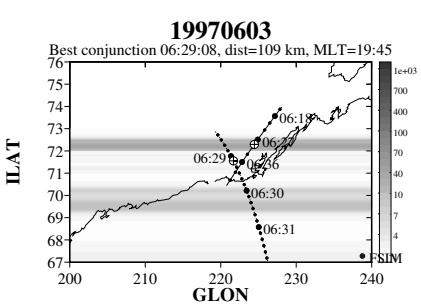
19970603
Best conjunction 06:29:08, dist=109 km, MLT=19:45
ILAT
GLON
06:18
06:29
06:30
06:31
FSIM

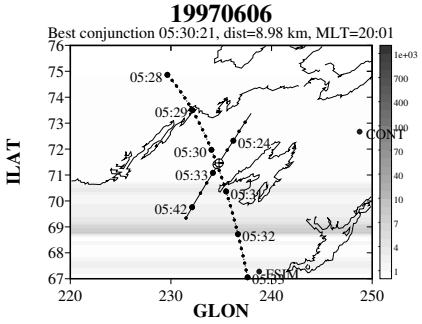
19970606
Best conjunction 05:30:21, dist=8.98 km, MLT=20:01
ILAT
GLON
05:28
05:29
05:30
05:24
05:33
05:42
05:32
CONT
FSIM

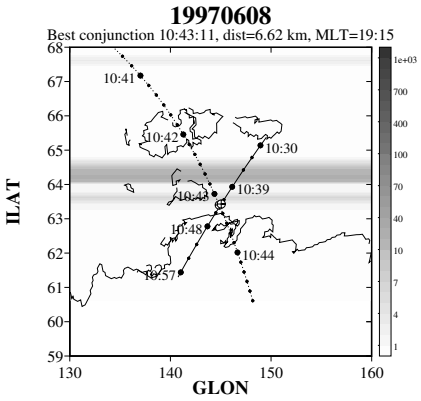
19970608
Best conjunction 10:43:11, dist=6.62 km, MLT=19:15
ILAT
GLON
10:41
10:42
10:30
10:39
10:48
10:44
10:57

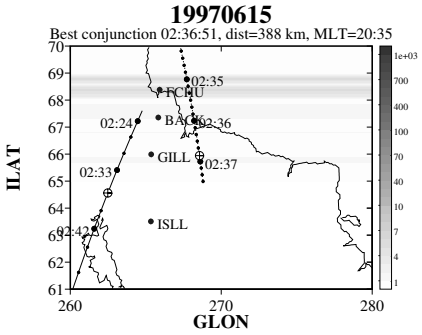
19970615
Best conjunction 02:36:51, dist=388 km, MLT=20:35
ILAT
GLON
02:35
FCRU
02:24
BAC
02:36
GILL
02:37
02:33
ISLL

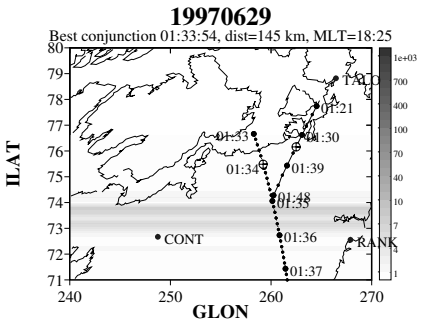
19970629
Best conjunction 01:33:54, dist=145 km, MLT=18:25
ILAT
GLON
01:21
01:33
01:30
01:34
01:39
01:48
01:35
CONT
01:36
RANK
01:37

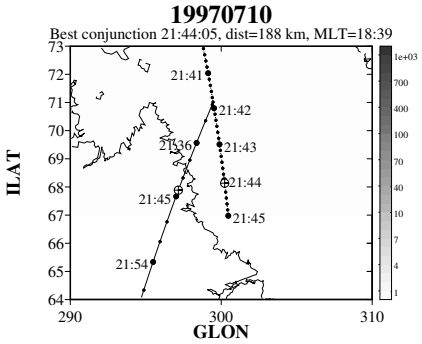
19970710
Best conjunction 21:44:05, dist=188 km, MLT=18:39
ILAT
GLON
21:41
21:42
21:36
21:43
21:44
21:45
21:45
21:54

Figure 3. Event maps for all inverted-V events and one diffuse event (970710). The equal-time minimum position of Polar (solid) and FAST (dotted) is shown with open circles. The energy flux of FAST in units of mW m^{-2} ($= erg\,cm^{-2}\,s^{-1}$) has been indicated in the plot by shading by assuming uniformity in the magnetic east-west direction. The horizontal axis shown is the geographic longitude to help locate the events on map, but the vertical axis is invariant latitude because the arcs are assumed to be aligned with that coordinate.

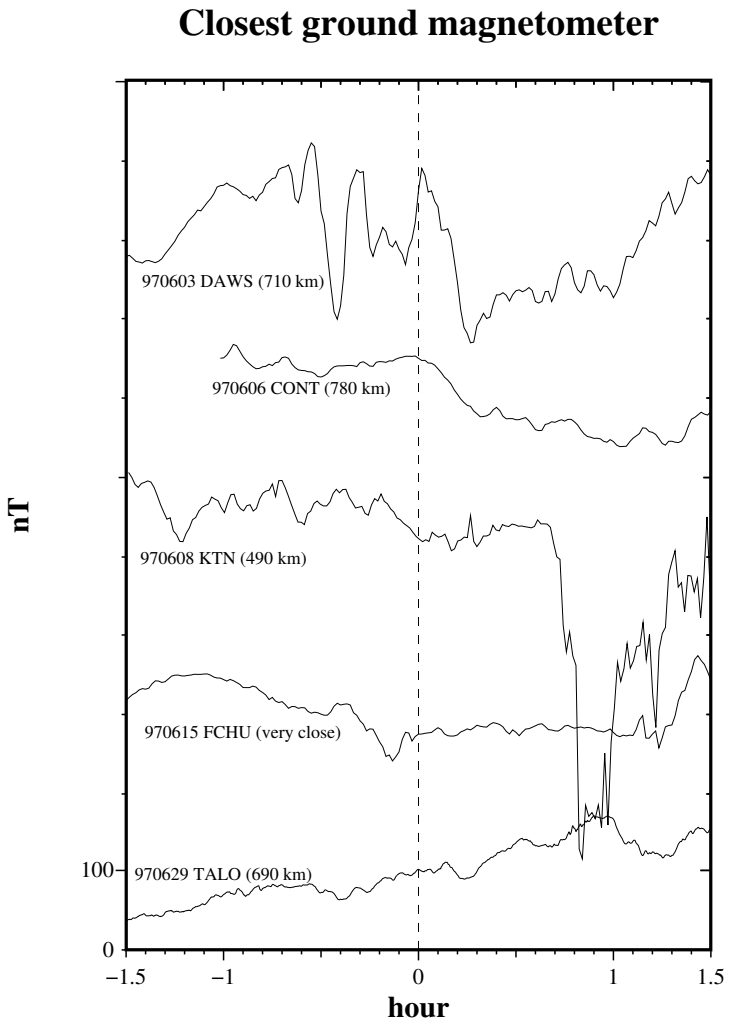

Figure 4. The closest ground magnetometer station X component in a 3-hour time window around each of the discrete precipitation events. Dawson (DAWS), Contwoyto Lake (CONT), Fort Churchill (FCHU) and Taloyoak (TALO) are CANOPUS stations, while Kotelny Island (KTN) station of the 210 MM chain belongs to the Institute for Cosmophysical Research and Aeronomy (IKFIA) of Russia. The time axis has been relabelled for each curve to make the time of best Polar/FAST conjunction equal to zero. An approximate distance from the conjunction point to the station is shown in parentheses.

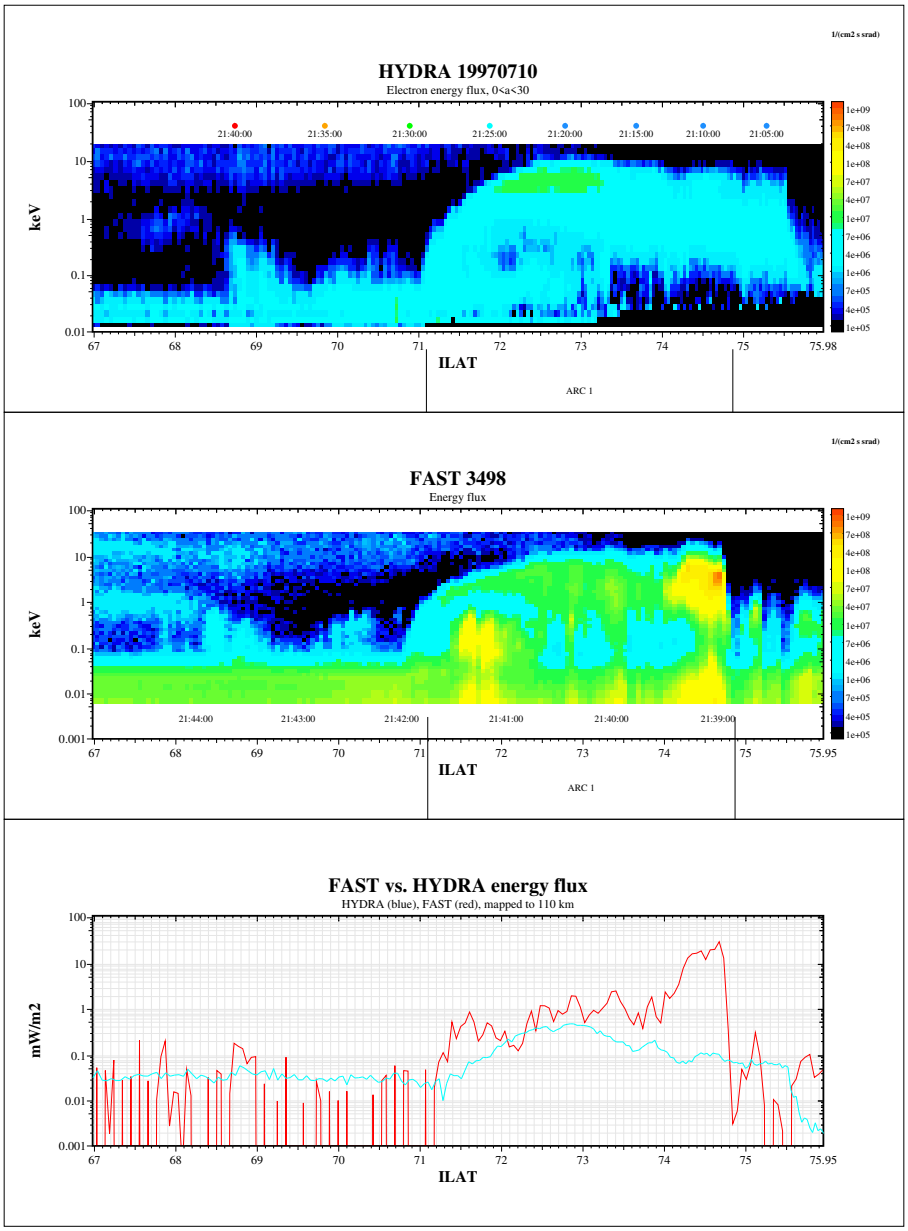
1/(cm2 s srad)
HYDRA 19970710
Electron energy flux, 0<a<30
keV
ILAT
ARC 1
FAST 3498
Energy flux
keV
ILAT
ARC 1
FAST vs. HYDRA energy flux
HYDRA (blue), FAST (red), mapped to 110 km
mW/m2
ILAT

Figure 5. HYDRA/FAST energy fluxes for 970710, which is a diffuse auroral event containing no inverted-V type precipitation at conjugacy. The upper panel shows HYDRA electron energy flux in the parallel direction (averaged from 0 to 30^o pitch angle). The time difference between HYDRA and FAST is indicated by red, orange, green, blue and dark blue dots corresponding to <5, 5-10, 10-15, 15-20 and >20 min time differences, respectively. The middle panel shows the corresponding quantity for FAST, mapped to the same invariant latitude. The arc is marked in the upper two panels. The third panel shows the integrated energy flux for both satellites mapped to the ionosphere. Despite some temporal difference, similar features can be recognized in FAST and HYDRA energy fluxes. FAST energy fluxes are about 2-3 times higher than HYDRA fluxes on the average in diffuse events.

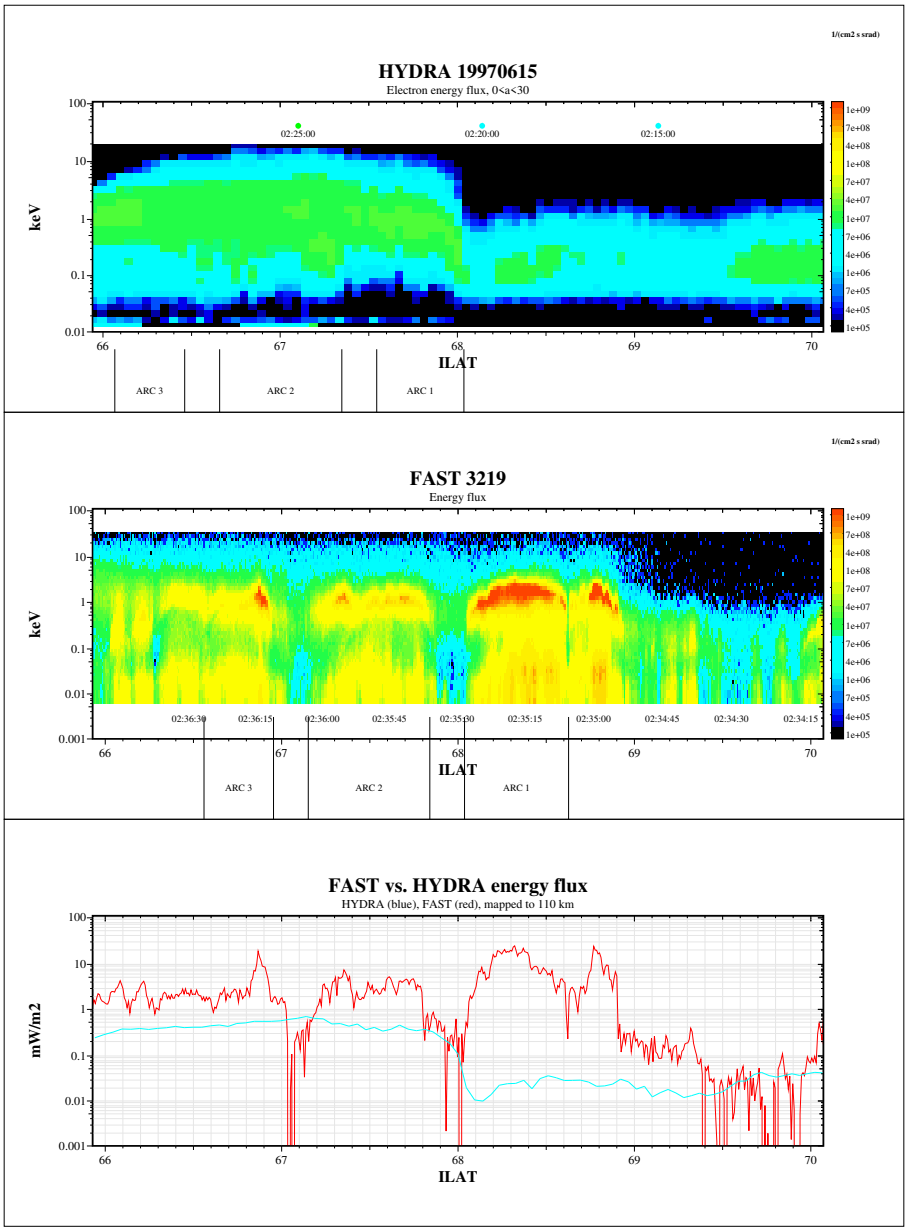

Figure 6. HYDRA/FAST energy fluxes for 970615, which is a quasi-Maxwellian inverted-V event. The panels correspond to those shown and explained in Figure 5. Here, however, the FAST energy flux is clearly larger than the HYDRA flux during discrete arcs. In further data processing of this event we have shifted FAST data by 0.6 degrees; it can be seen that this improves the matching of the panels. The shift means that the arc orientation probably differs somewhat from east-west orientation in this event.

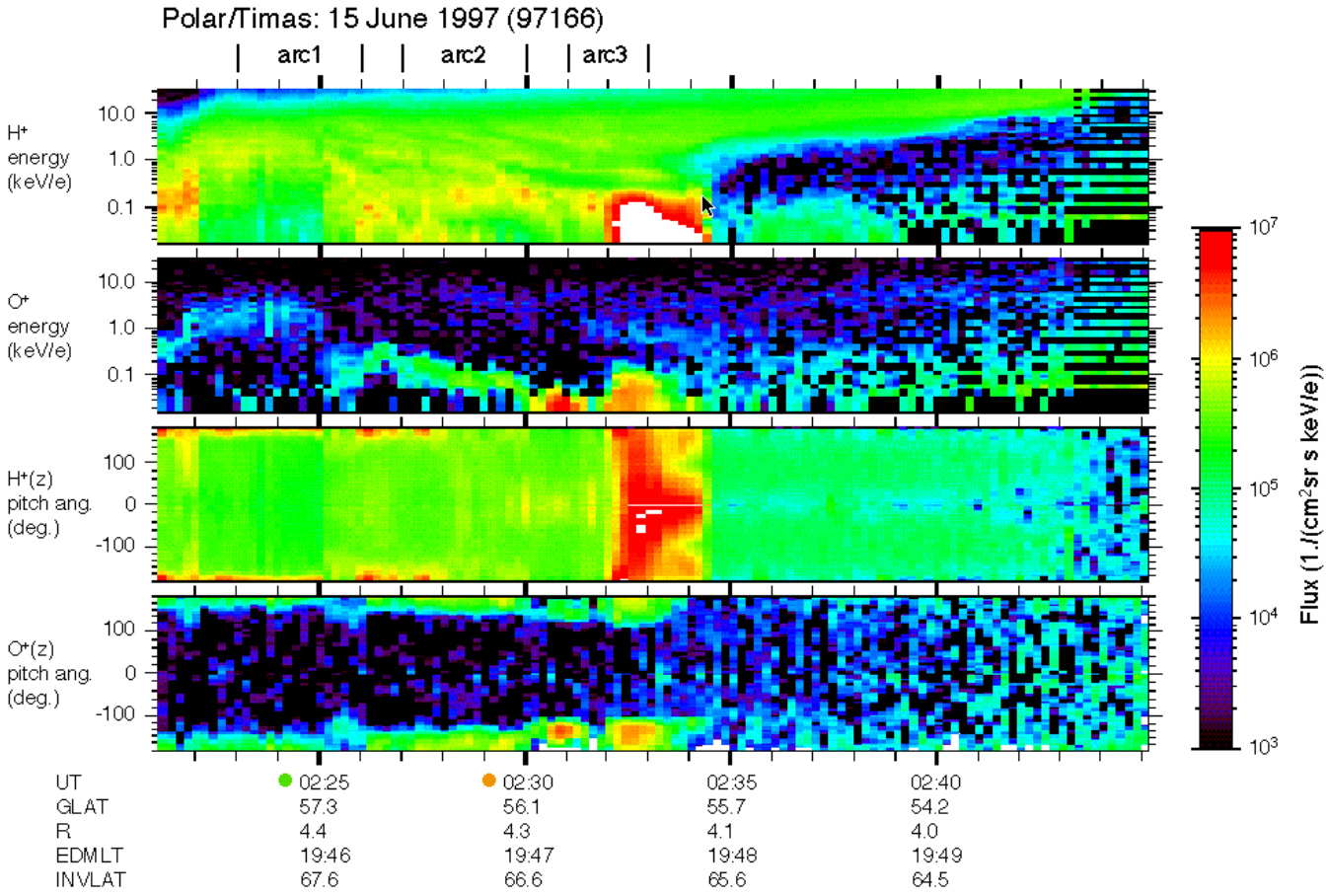

Figure 7. TIMAS energy-time spectrograms and pitch angle distributions for the energy range 0.015 .. 12 keV for 970615, showing hydrogen and oxygen ions.

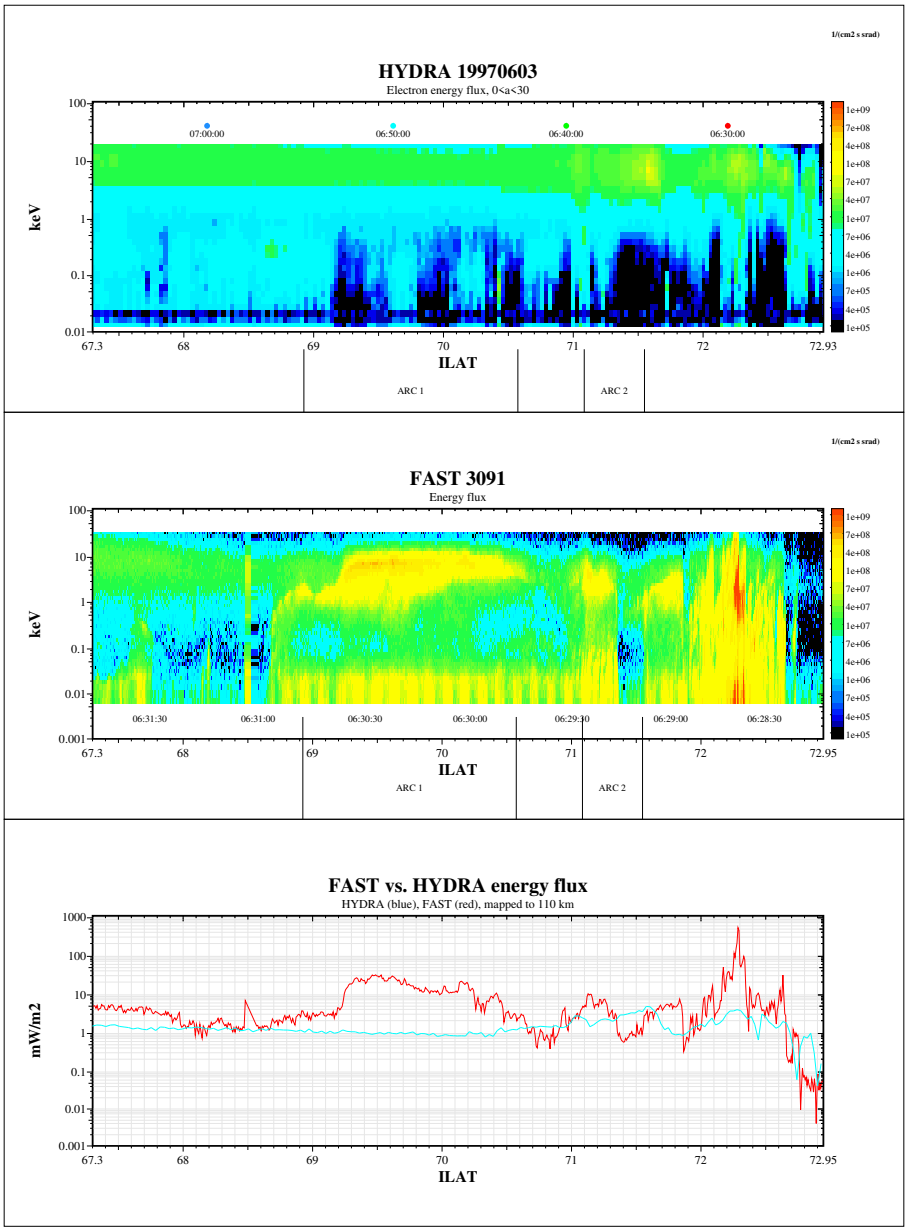

Figure 8. HYDRA/FAST energy flux for 970603 (same format as Figure 6). When inverted-V precipitation is seen, FAST energy flux is about 10 times higher than HYDRA.

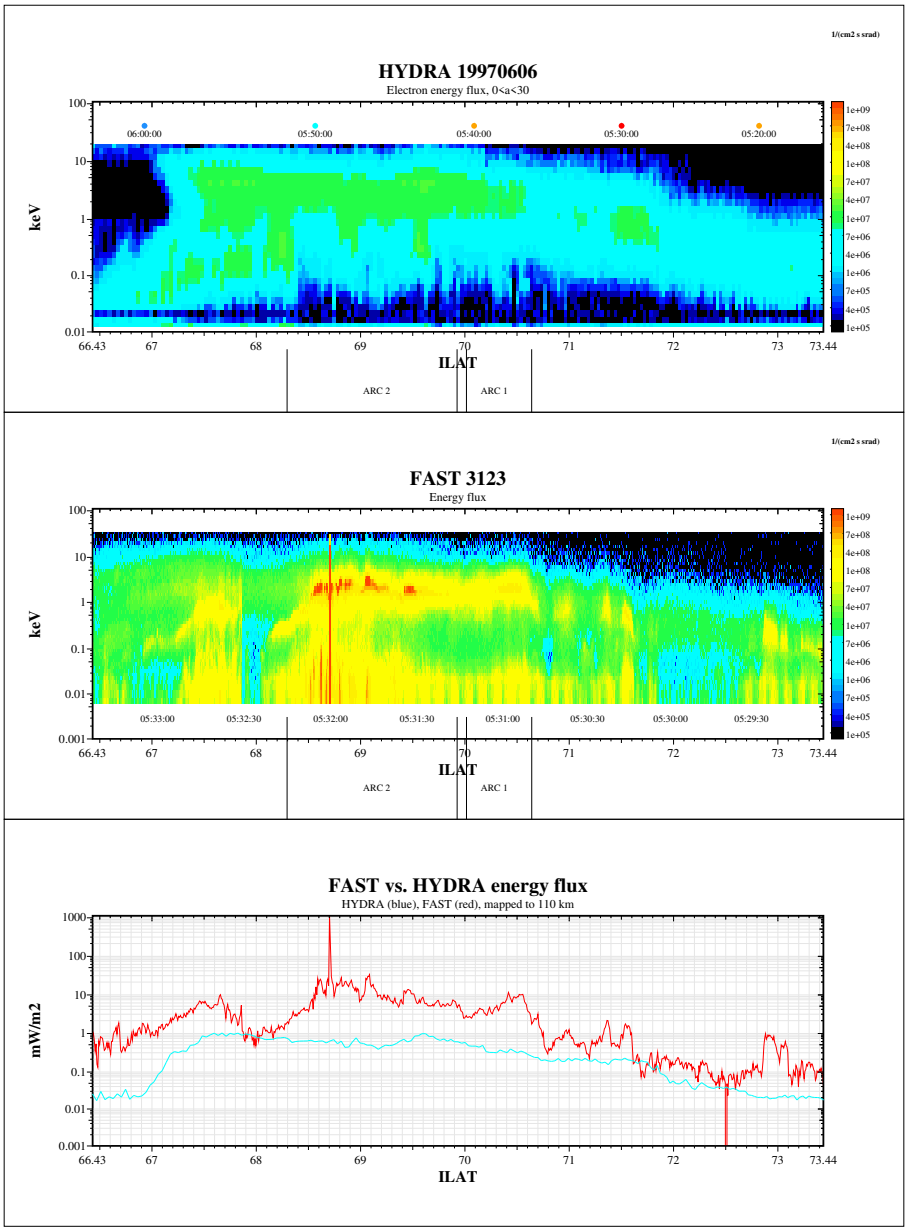

Figure 9. HYDRA/FAST energy flux for 970606 (same format as Figure 6).

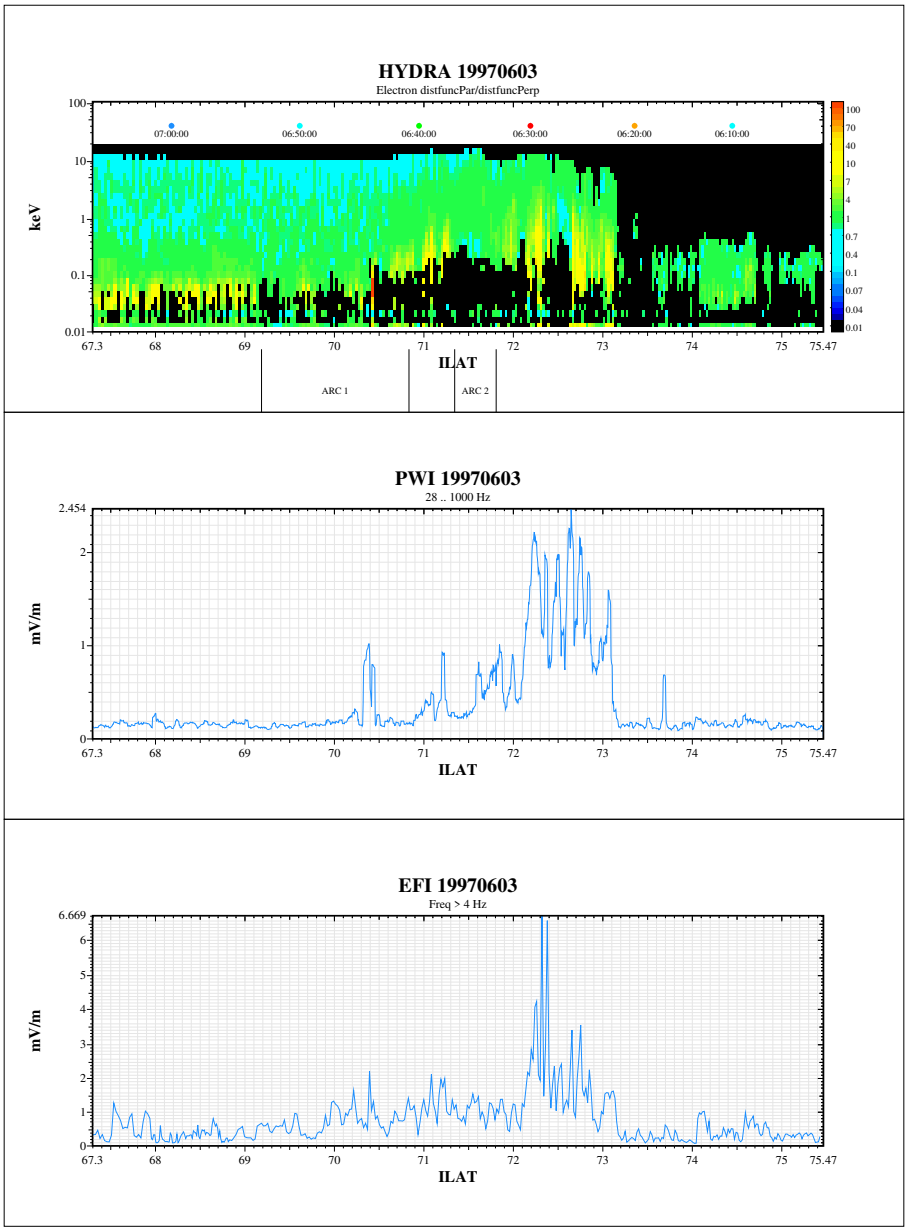

Figure 10. Upper panel: HYDRA parallel vs. perpendicular anisotropy ($f_{\parallel}/f_{\perp}$). Middle panel: PWI electric wave activity between 28 Hz (the lower threshold of the instrument) and 1 kHz (a limit above which the broadband activity starts to fade and other wave phenomena might interfere) from the "U" antenna. Lower panel: EFI instantaneous electric field amplitude in the 4-10 Hz frequency range. $f_{\parallel} > f_{\perp}$ anisotropies are seen to be correlated with waves, for example, at 70.4 ILAT. The PSI instrument is operating during this event, so PWI and EFI data must be used very cautiously. There is no reason why the correlation could be caused by PSI, however.

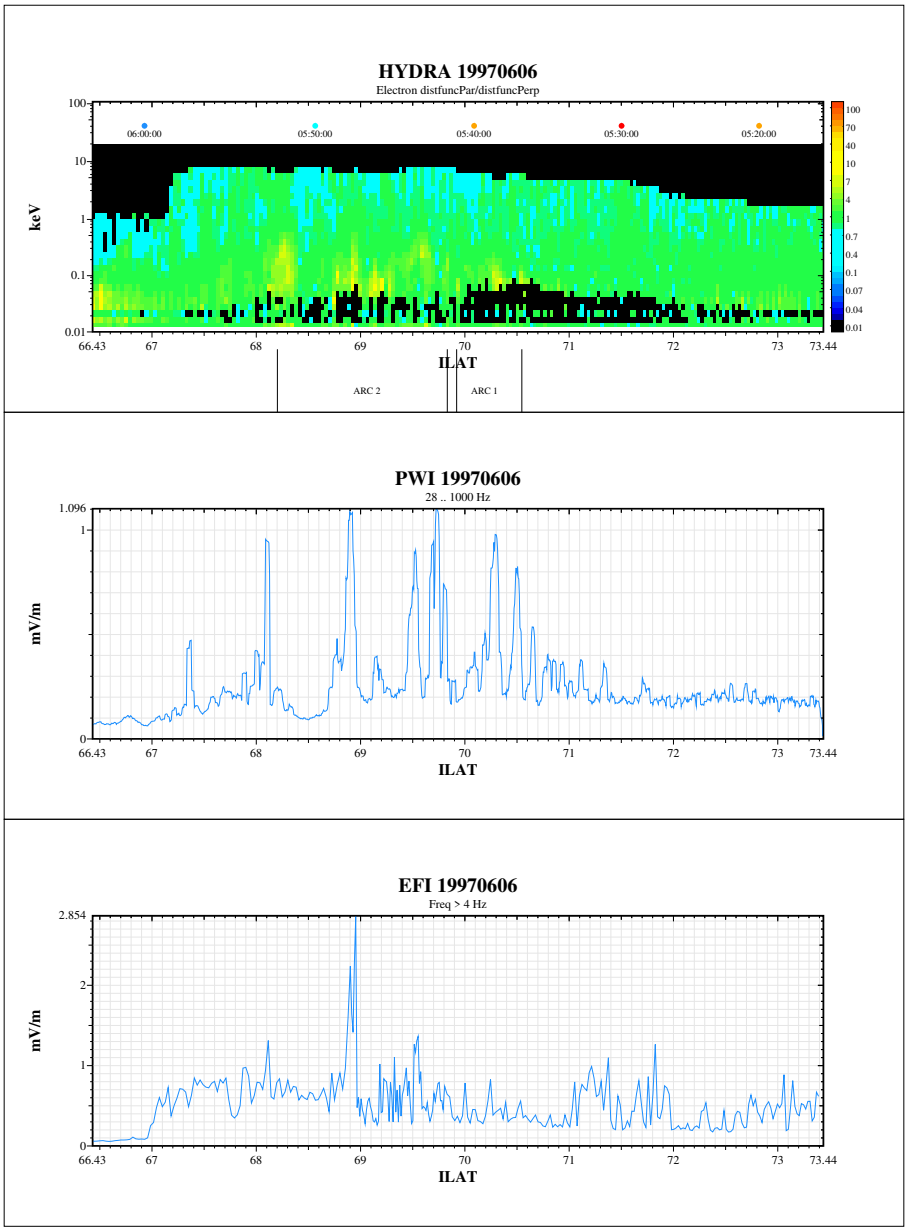

Figure 11. Anisotropy and wave amplitudes for 970606 (same as Figure 10). Also here the $f_{\parallel} > f_{\perp}$ anisotropies (yellow and red) are correlated with waves. PSI is on in this event as well.

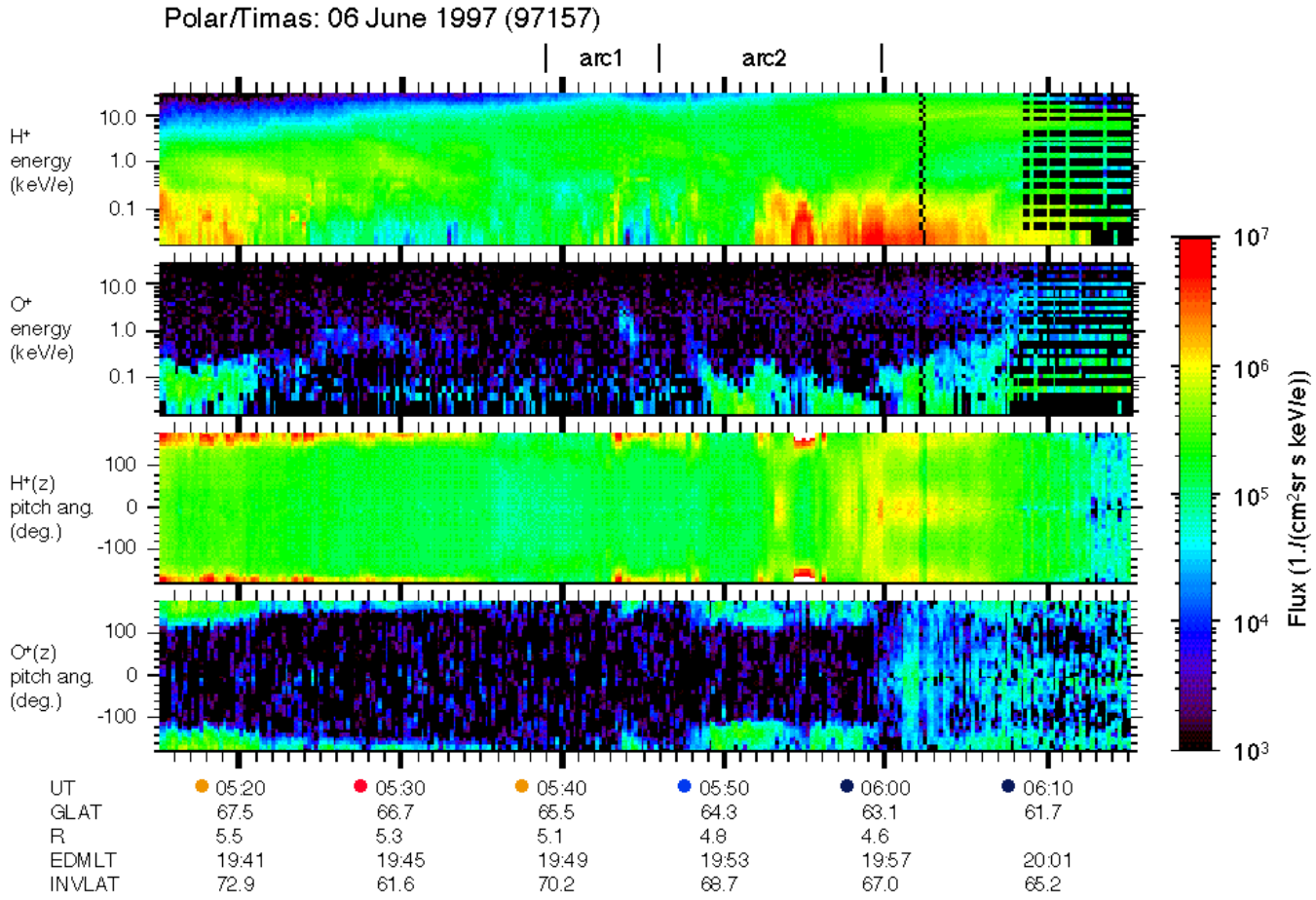

Figure 12. TIMAS ion data for 970606 (same as Figure 7).

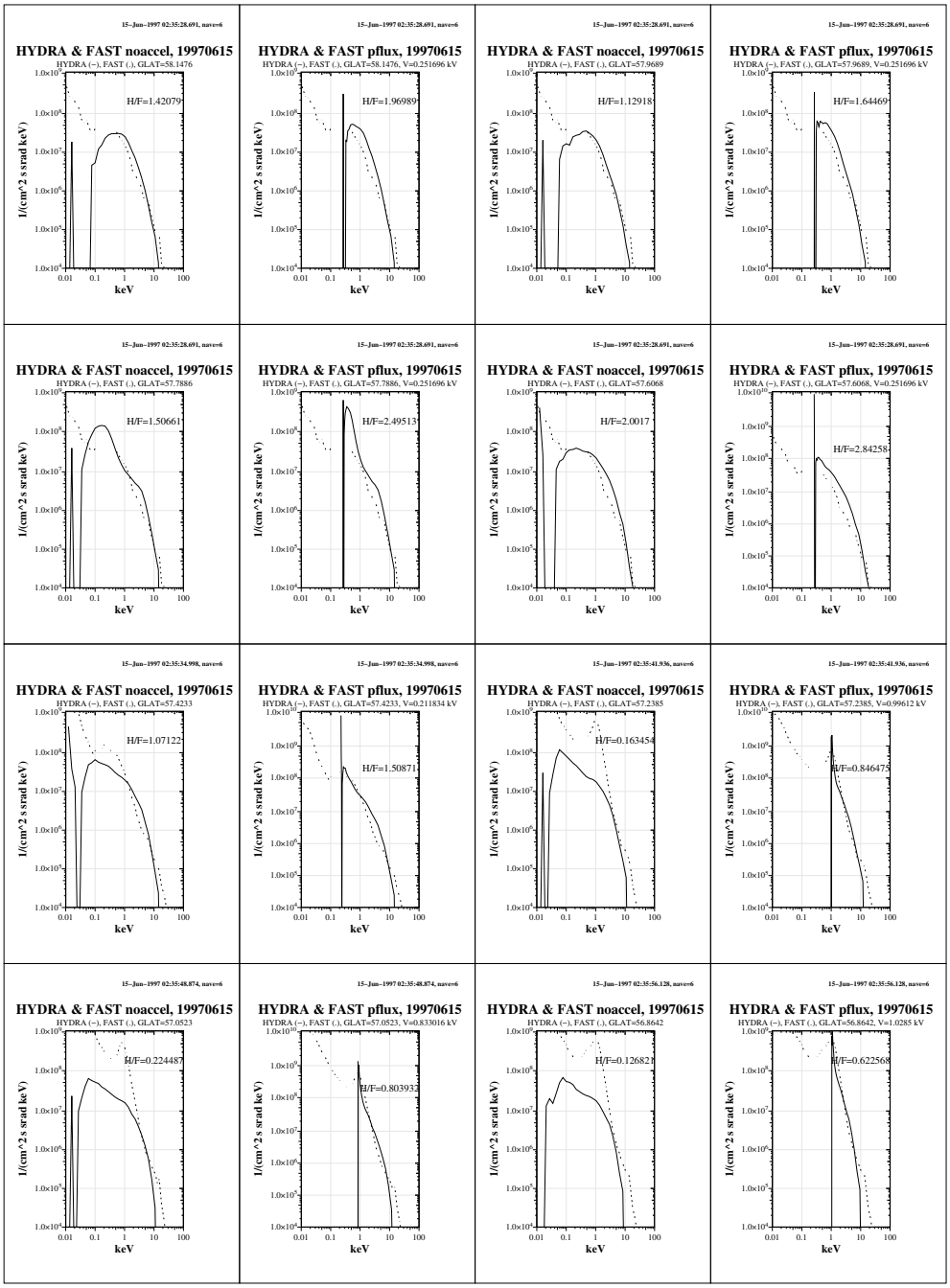

Figure 13. HYDRA (solid) and FAST (dotted) particle fluxes for 970615 (a quasi-Maxwellian event). The plot contains 8 pairs of nonaccelerated/accelerated line spectra, selected uniformly during inverted-V precipitation. The accelerating voltage has been found from the peak position of FAST (with 0.6 degree latitudinal shift). We see that the nonaccelerated HYDRA spectra are mostly quasi-Maxwellian. After acceleration, the correspondence with FAST is good in this event.

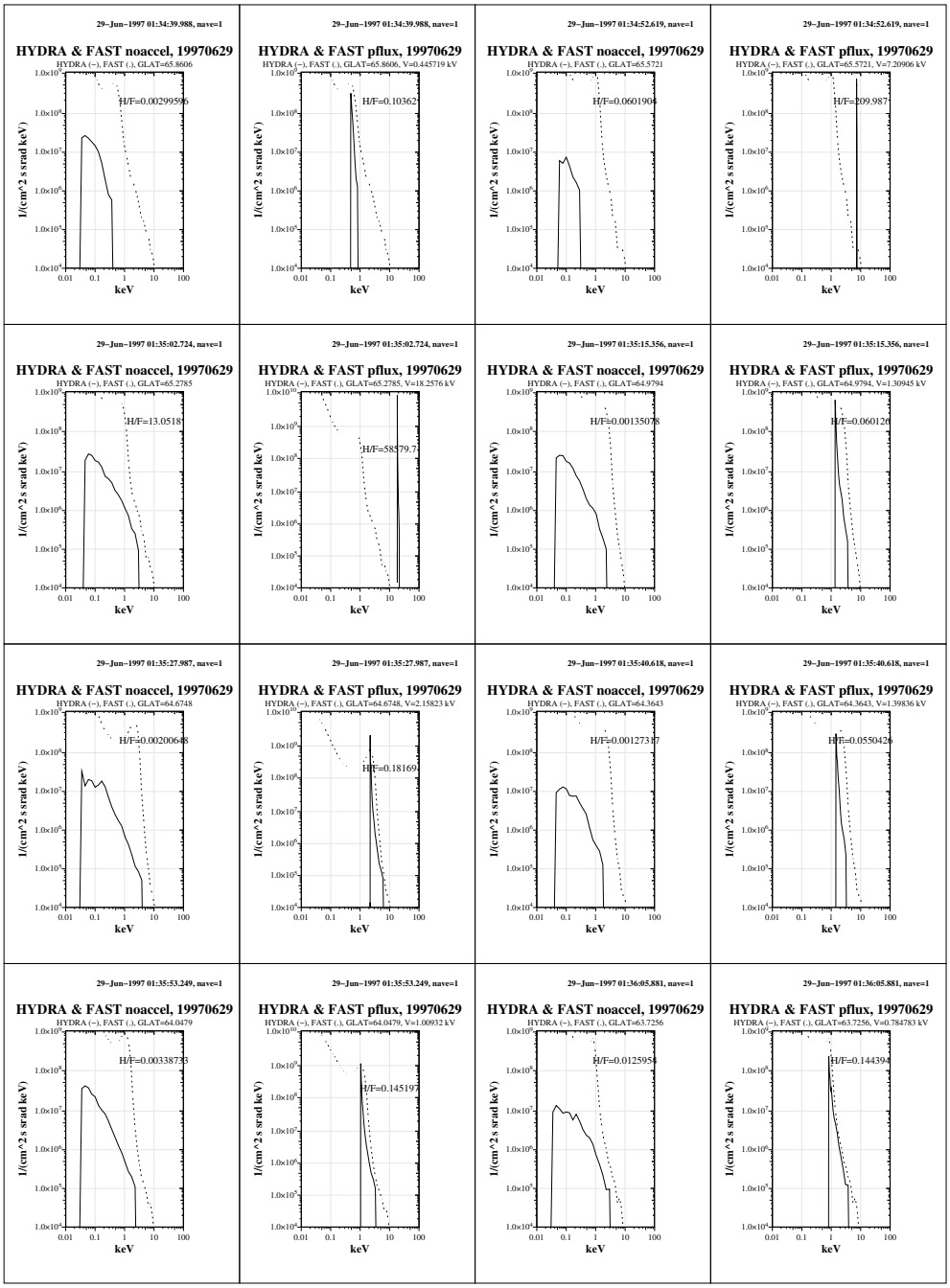

Figure 14. Same as Figure 13 but for 970629. No latitudinal shifting is done in this event. In some cases the automatic peak position finding algorithm finds the wrong peak (for example, the top-right plot).

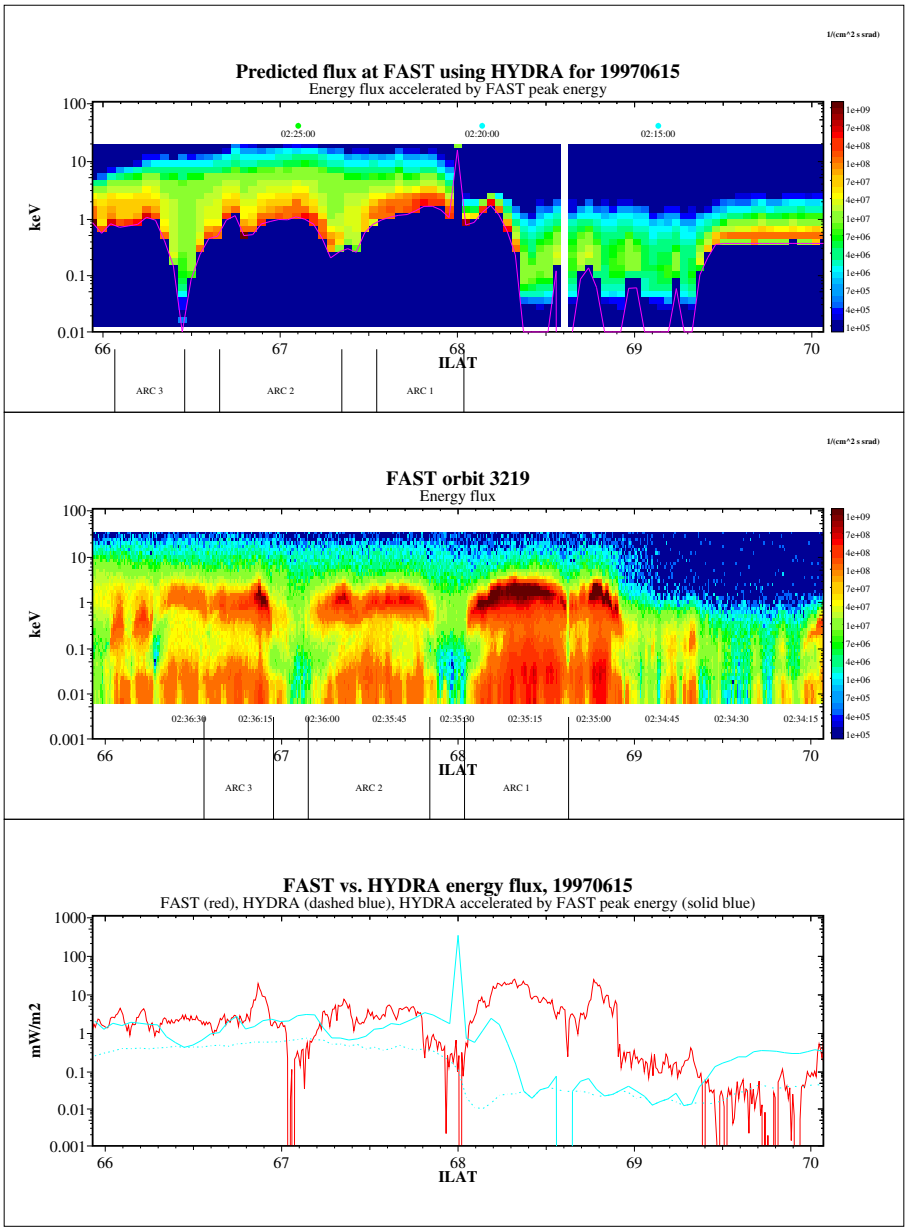

Figure 15. Top panel: HYDRA electron energy flux accelerated by FAST peak energy (simulated effect of parallel potential drop). A latitudinal shift of 0.6 degree was included when finding the FAST peak energy. Middle panel: FAST energy flux. Bottom panel: Comparison of FAST energy flux (red) with HYDRA accelerated energy flux (blue). The originally measured HYDRA energy flux (nonaccelerated) is also shown (dotted blue).

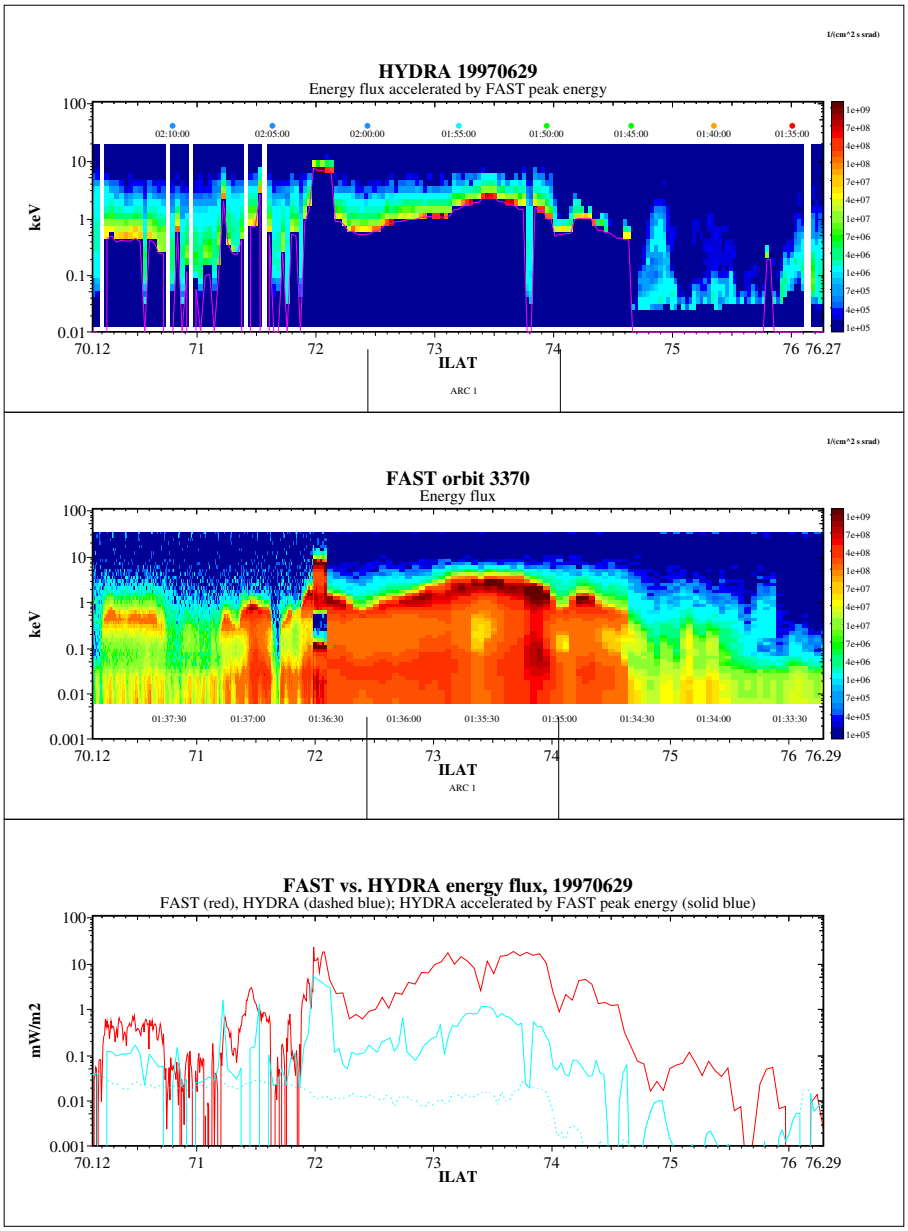

Figure 16. Same as Figure 15, but for 970629. No latitudinal shifting in this event.

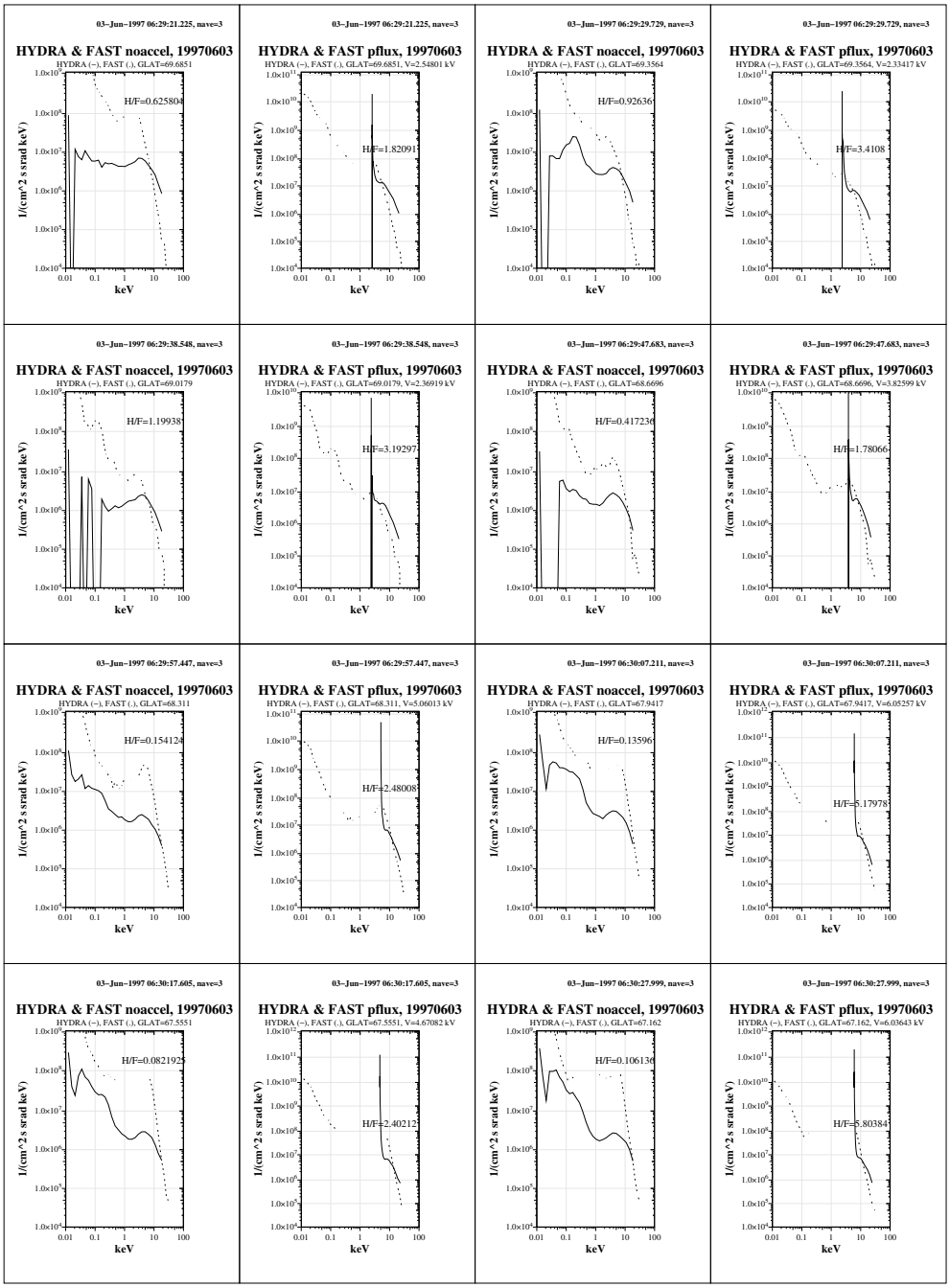

Figure 17. Same as Figure 13 but for 970603, where HYDRA data are of the non-Maxwellian type.

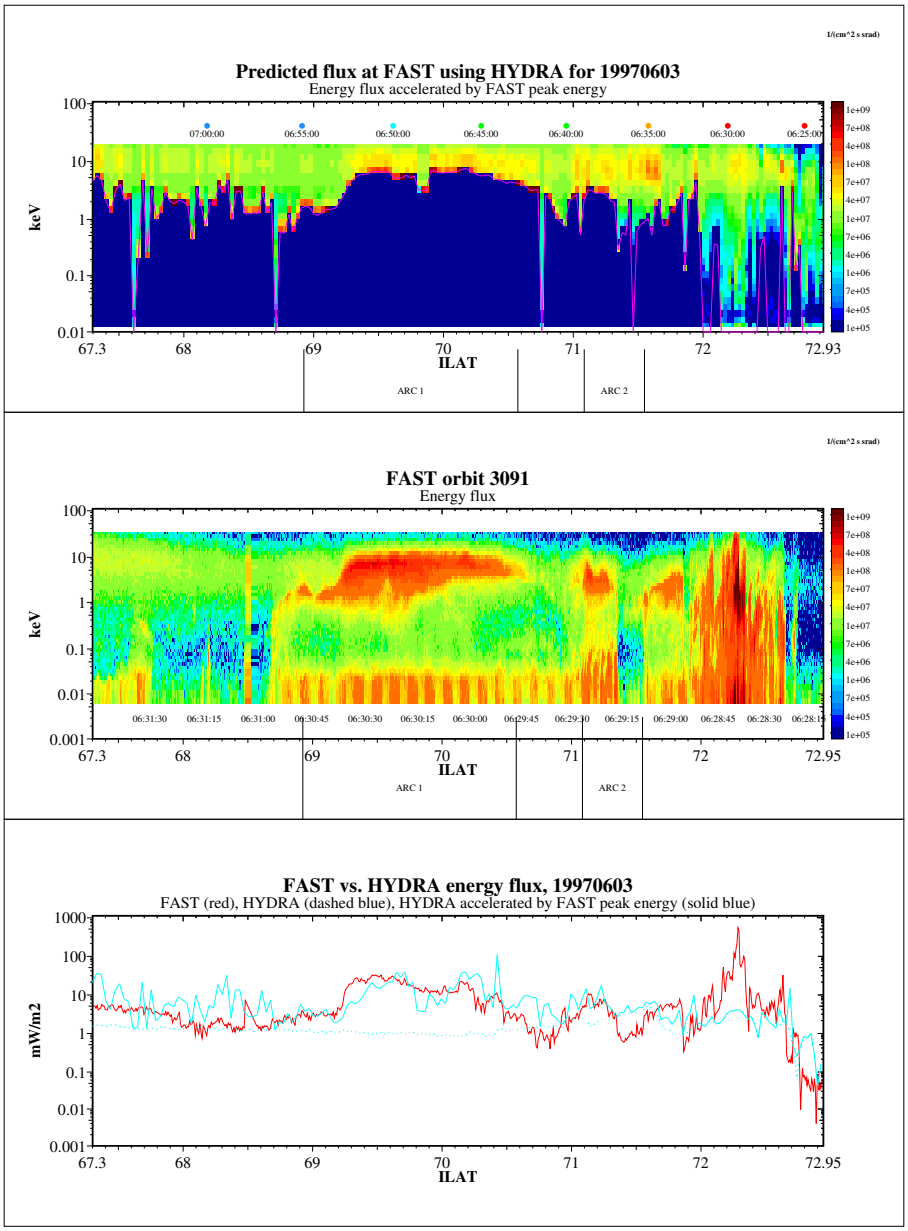

Figure 18. Same as Figure 15 but for 970603, where HYDRA data are of the non-Maxwellian type.

Table 1. The FAST/Polar auroral conjunctions

Date	UT	MLT	FAST alt	Polar alt	Dist	Inv-V	PSI
970603	06:30	19:30	1900	30000	109 km	Yes/NM	On
970606	05:31	20:00	2200	26000	9 km	Yes/NM	On
970608	10:43	18:30	2100	26000	7 km	Yes/NM	On
970615	02:35	20:30	3100	20000	388 km	Yes/QM	Off
970629	01:35	18:40	3600	27000	145 km	Yes/QM	Off
970710	21:39	18:30	4100	24000	188 km	No	Off
970720	16:22	05:20	3200	29000	62 km	No	Off
980727	06:40	06:40	2800	35000	54 km	No	On
980811	02:58	04:15	3400	37000	163 km	No	Off

Each FAST auroral traversal lasts about 2 minutes; the universal and mean local times given are approximately at the center of each event, or when the most important arcs were seen. The minimum equal-time distance of the footpoints in the ionosphere is also given. In five events, inverted-V arcs were seen. In 970615 and 970629, HYDRA electron spectra is of quasi-Maxwellian (QM) rather than non-Maxwellian (NM) type most of the time. The Plasma Source Instrument (PSI) [*Moore et al.,* 1995] onboard Polar is operating in four events so that low-energy particle, electric field and wave measurements may be affected and have to be interpreted with care. The last four events were diffuse precipitation events.